IMPEDANCE AND BEAM INSTABILITY ISSUES AT J-PARC RINGS

Y. H. Chin, K. Takata, and A.Toyama, KEK, Tsukuba-shi, Ibaraki-ken, Japan
Y. Shobuda and J. Kamiya, JAEA, Tokai-mura, Ibaraki-ken, Japan

Abstract

In this paper, the dominant impedance sources in the J-PARC rings (RCS and MR) are discussed, and their effects on beam instabilities are estimated. They are the kicker magnets at the both rings and the stainless-steel chamber at the MR ring. Some damping methods of kicker impedances are introduced and experimental results to asses their effectiveness are described. A new estimate of the resistive-wall impedance of the MR stainless-steel chamber, based on the Zotter-Métral formula, reveals that the resistive-wall impedance is actually doubled, compared to the previous estimate based on the classical formula. Development of a damper system using the existing exciters for tune measurements is also described.

ISSUES OF CONCERNS

The layout of the J-PARC facilities is shown in Fig. 1[1]. It consists of the 181MeV linac, the 3GeV Rapid-Cycling Synchrotron (RCS) operated at 25Hz, and the 50GeV Main Ring (MR) synchrotron operated at 0.3Hz. The RCS provides 3GeV proton beams to the Material and Life Experimental Hall for neutron spallation. The MR provides 30-50 GeV proton beams to the Hadron Experimental Hall for hadron physics and to the neutrino beam line to send neutrino beams to the Kamiokande facility located in 300km away Kamioka. The main parameters of the RCS and MR rings are summarized in Tables 1 and 2, respectively.

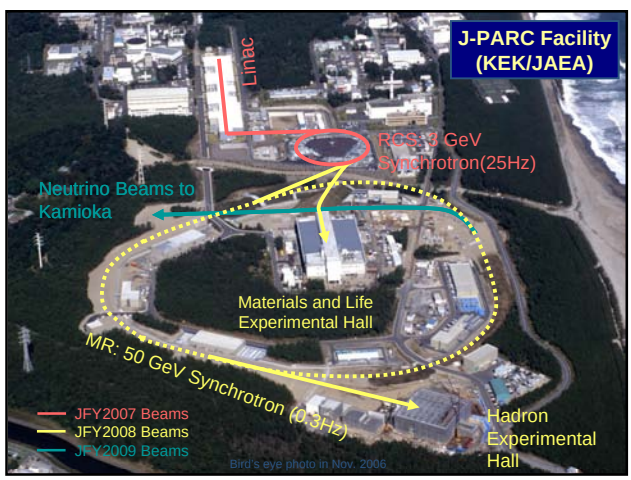

Figure 1: The layout of the J-PARC facilities.

At the both rings, the sharp impedances of kicker magnets are expected to cause beam instabilities at the beam power of around a few 100kW. Study and testing of several damping methods of kicker impedances are under way. At the MR, the resistive-wall impedance of the stainless-steel chamber is another dominant source for transverse beam instabilities. Recent study shows that the previous estimate of the resistive-wall impedance using the classical formula [2] is rather inaccurate: the skin depth of the stainless-steel chamber at the first unstable betatron frequency line is comparable with the thickness of the chamber itself, and therefore the classical formula for the resistive-wall impedance may be out of applicable range. More precise estimates of the chamber impedance and the beam instabilities have been done. We are also working on development of a transverse damper system for damping of transverse beam instabilities, using the existing two exciters installed at the MR for transverse tune measurements (horizontal and vertical, respectively).

Table 1: Main Parameters of the RCS (C=348.3m, h=2, Repetition Rate=25Hz)

Kinetic energy (GeV)	0.181	3
Revolution frequency (MHz)	0.47	0.84
Slippage factor	-0.69	-0.047
Q_x/Q_y	6.68/6.27	
Bunching factor	0.374	0.185
Protons/bunch/10^{13}	2.49	4.15
Average current (A)	3.74	11.1
Peak current (A)	10	60
$\Delta p/p$ (%)	0.85	0.38
Half bunch length (m)	55	20
Synchrotron tune	0.0058	0.0005

Table 2: Main Parameters of the MR (C=1567.5m, h=9, Repetition Rate=0.3Hz)

Kinetic energy (GeV)	3	50
Revolution frequency (MHz)	0.186	0.191
Slippage factor	-0.058	-0.0013
Q_x/Q_y	22.33/22.28	
Bunching factor	0.336	0.056
Protons/bunch/10^{13}	4.15	4.15
Average current (A)	9.86	10.2
Peak current (A)	29.3	182
$\Delta p/p$ (%)	0.85	0.25
Half bunch length (m)	41	8
Synchrotron tune	0.0025	0.0001

KICKER IMPEDANCES

Impedance Measurements

Figure 2 shows the measured horizontal impedance of a RCS prototype kicker magnet. For comparison, the vertical impedance of a SNS kicker magnet [3] is shown

in Fig. 3. The RCS kicker has many sharp peaks over several MHz, and they reach around 35,000 Ω/m. On the other hand, the SNS kicker has much smoother impedance and the impedance peaks are lower than 2,500 Ω/m. The sharp peaks in impedances are due to cable resonances of beam-induced currents in the kicker magnet. The reason of this factor of 10 differences is that the SNS kickers use saturable inductors to damp these cable resonances [4]. Its scheme is illustrated in Fig. 4. The saturable inductor behaves as low impedance for high-current pulses from the modulator, while it behaves as high impedance for the resonant current induced by a beam and lets this current flow through the resistor to damp. This scheme is plausible only for lumped constant type kickers.

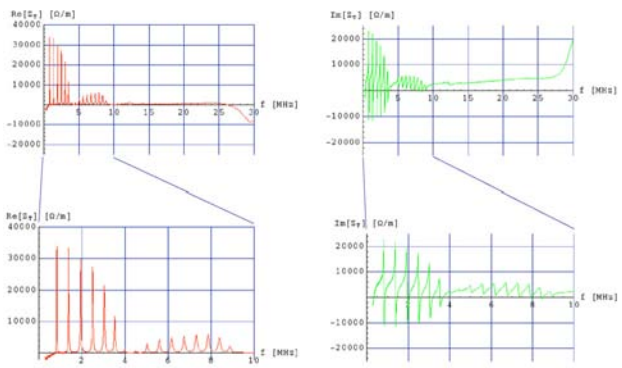

Figure 2: Measured horizontal kicker impedance of the RCS prototype kicker magnet.

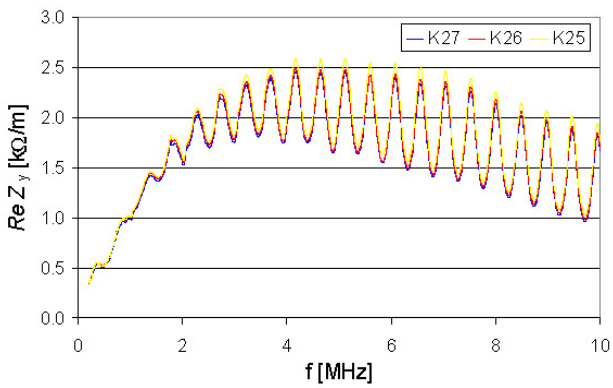

Figure 3: Measured vertical impedance of the SNS kicker magnet [3].

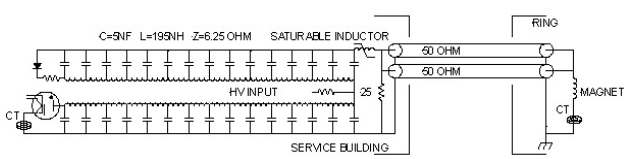

Figure 4: Simplified schematic diagram of the SNS modulator with a saturable inductor for damping of kicker impedances [4].

A question is whether we can use the same scheme to damp the cable resonances at the MR and RCS. In the MR, the answer seems to be yes, since all existing kicker magnets will be renewed to the lumped constant type for improvement of kicker performance anyway. Indeed, study is under way for that end. However, such scheme seems to be no option for the RCS where the existing distributed constant type kicker magnets will be continuously used for some time in future.

Horizontal Instability Evaluation

Figure 5 shows the calculated growth rate of horizontal beam instabilities due to the kicker impedances at the MR, as a function of the ramping time. The chromaticity is assumed to be perfectly corrected to zero at any energy. This calculation is based on the linear theory where no dumping effect due to non-linear effects such a betatron tune spread is considered. The horizontal growth rate is rather large and serious at low energy, in an order of several 100Hz. This result indicates that the impedance resonances in the kicker cable need to be damped for stable operation of the MR.

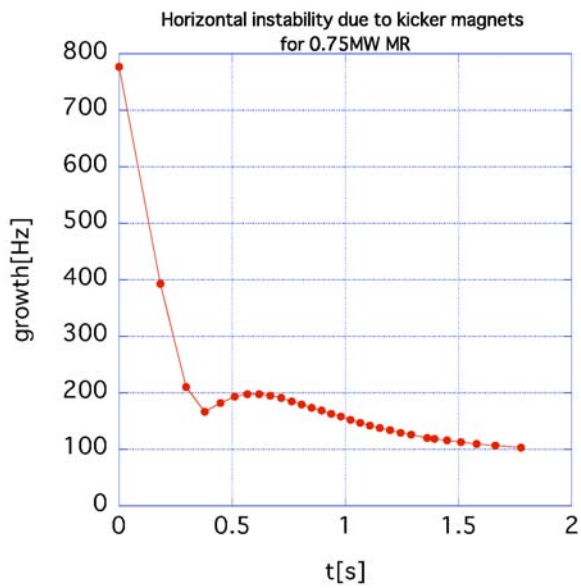

Figure 5: The calculated growth rate of horizontal beam instabilities due to the kicker impedances at the MR as a function of the ramping time, for the zero chromaticity case.

For more accurate estimates of horizontal instabilities, beam instability simulations need to be carried out, using realistic simulation codes such as ORBIT [5]. The ORBIT code and many templates for input files have been installed to both the KEK and JAEA parallel computers, thanks to the collaboration with the Oakridge National Laboratory. However, actual runs are still under preparation stage.

Damping of Cable Resonances

An experiment was done to confirm that the sharp peaks in the kicker impedances are really caused by cable resonances, and to demonstrate that they can be damped in principle using resistors, similar to the SNS kicker system, but placed in a different position (see Fig. 6). The kicker impedance was measured with/without the resistors and for various conditions at the end of kicker cable. The measurement results are shown in Fig. 7.

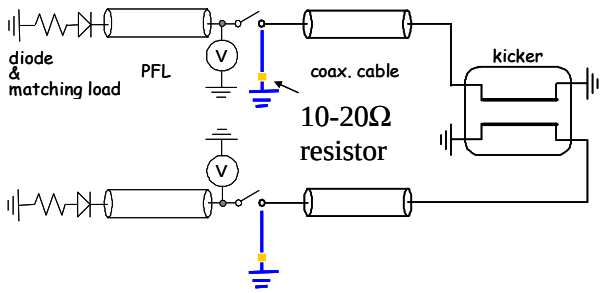

Figure 6: The experimental set-up for damping of cable resonances.

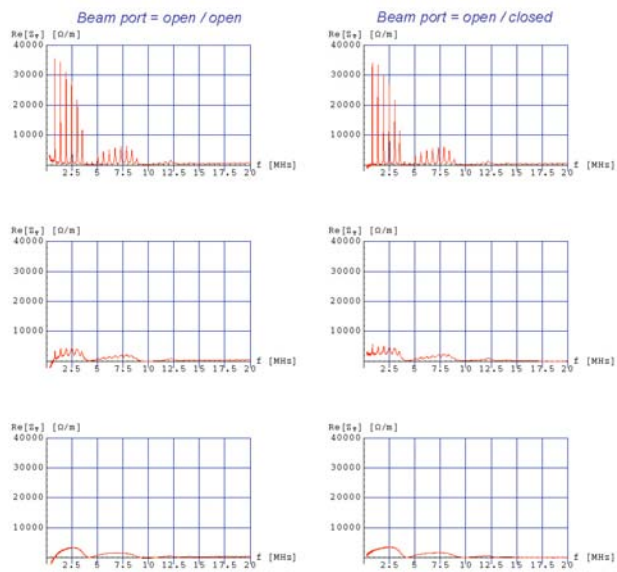

Figure 7: Measured kicker impedance with/without the resistors and for various conditions at the end of kicker cable.

The top figures show the impedances when the cable end is open without the resistors. The sharp peaks of impedances are visible. The middle figures show the impedances when the cable end is connected with the resistors of 20Ω. The sharp peaks are almost smoothed out. The bottom figures show the case that the cable itself is disconnected from the kicker and the resistors of 10Ω are directly attached to the kicker magnet. The remaining small peaks are completely removed. These results prove that the sharp peaks in the kicker impedances are cable resonances and they can be damped in principle using resistors. However, we need a mechanism to isolate the damping resistors from pulse current from the modulator to the kicker. Several ideas for such isolation have been proposed using diodes or solid-state switches. However, they have some engineering difficulties and no idea was validated yet.

Absorbers in Kicker Magnet

Meantime, more direct approaches using absorbers in the kicker magnet have been tested. One idea is to use a lossy material such as graphite (the bulk conductivity $=10^5/\Omega$m) for the flux break. Another idea is to wrap up (or cover interior of) the kicker ferrite with an absorber such as SiC, which does not affect the magnetic fields inside the ferrite core but damps only the electric wake-fields. These ideas are illustrated in Fig. 8.

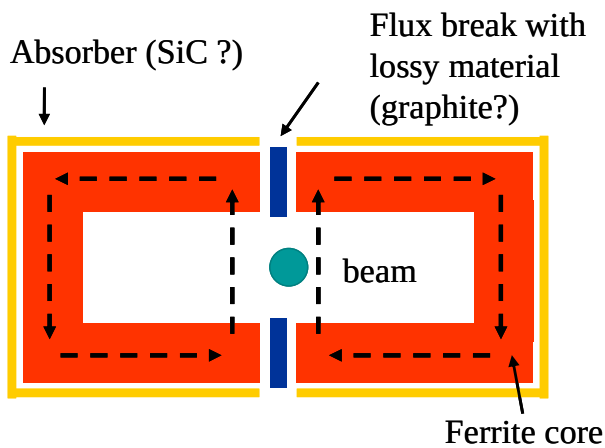

Figure 8: Illustration of absorbers in the kicker magnet.

Test of Principle

We replaced the upper flux break of the RCS kicker prototype by a graphite plate, and measured both longitudinal and transverse impedances. The actual set-up with the graphite plate as the upper flux break is shown in Fig. 9.

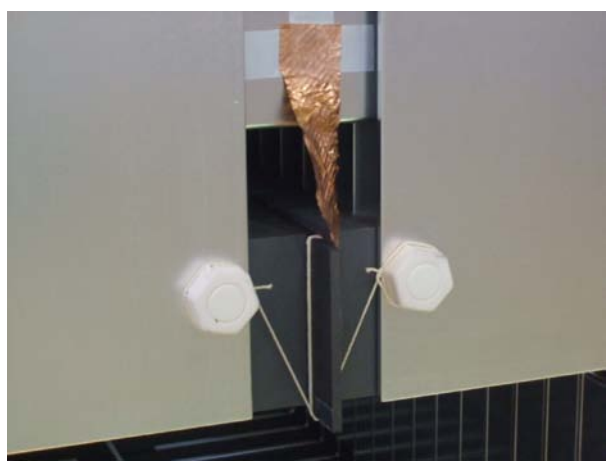

Figure 9: The actual set-up with the graphite plate as the upper flux break.

The measured real part of the longitudinal impedance is shown in Fig. 10. It can be seen that the impedance is actually halved by the absorber effect. The measure real part of horizontal impedance, however, shows a little sign of reduction, as can be seen in Fig. 11. These results indicate that the lossy flux break has some effects to reduce the longitudinal impedance of kicker, while it has only a small effect (5-10%) on the horizontal impedance.

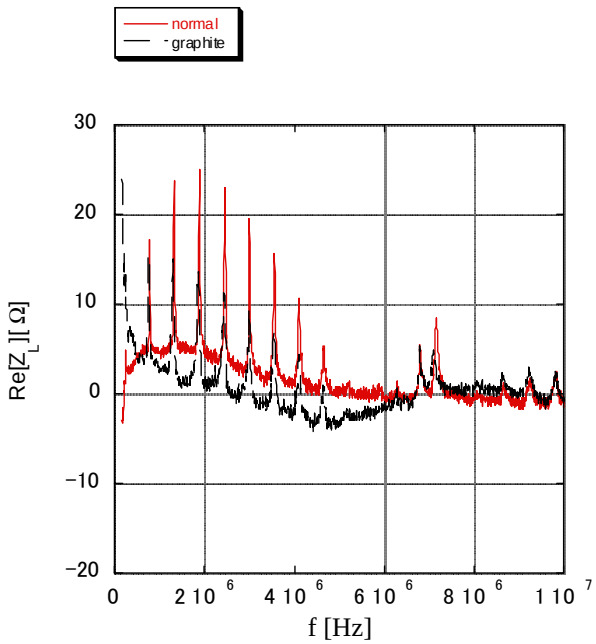

Figure 10: The measured real part of the longitudinal impedance with the graphite plate as the upper flux break.

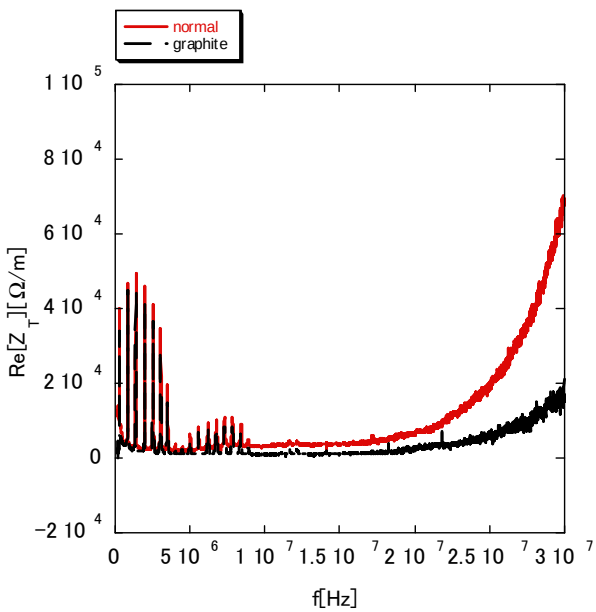

Figure 11: The measured real part of the horizontal impedance with the graphite plate as the upper flux break.

RESISTIVE-WALL IMPEDANCE OF MR STAINLESS-STEEL CHAMBER

The stainless-steel chamber used at the MR is another dominant source of the transverse impedance and corresponding transverse beam instabilities. The estimated growth rate of the vertical beam instabilities can reach almost 1 kHz at the injection energy of 3 GeV, when the chromaticity is corrected to zero.

This result is based on the calculation of the resistive-wall impedance of the stainless-steel chamber using the classical formula [2], where the skin depth is assumed to be much smaller than the thickness of the chamber wall. However, the stainless-steel chamber of the MR has typically a diameter of 120cm and thickness of 2mm. The first unstable betatron frequency line is around 50–60 kHz. At this frequency, the skin depth of the stainless-steel chamber is about 2mm, comparable with the thickness of the chamber itself. Questions arise:

(1) Can wake-fields leak out of the chamber, since the chamber is not thick enough, compared to the skin depth?
(2) If so, was the previous calculation of the resistive-wall impedance of the chamber based on the classical formula an overestimate?

There are renewed interests in the resistive-wall impedance at the LHC [6, 7] where the skin depth (=18mm) at the first unstable betatron oscillation frequency (=8kHz) in the LHC graphite collimators (25mm thick) is much larger than the aperture of the graphite collimator (2mm apart), and thus the classical formula of the resistive-wall impedance is out of applicable range.

Zotter and Métral developed new theories of the resistive-wall impedance for such case [6, 7]. According to their theories, the transverse resistive-wall impedance of the LHC graphite collimators becomes linear to the frequency, ω, at low frequency, instead of the usual $1/\omega^{1/2}$ dependence. Such behavior is shown in Fig. 12.

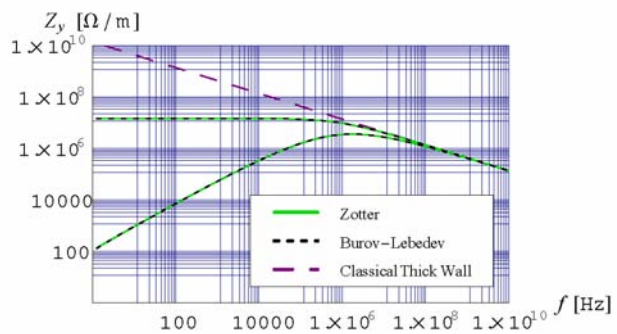

Figure 12: Transverse impedance of the LHC graphite collimators [6].

Using the new Zotter-Métral formula [6, 7] assuming open air outside of the chamber, we found that the

transverse impedance of the MR stainless-steel chamber becomes even larger at the first unstable betatron frequency line than the previous estimate. The entire frequency dependency of the transverse impedance of the stainless-steel chamber is plotted in Fig. 13. There are three different regions in the impedance curve. At high frequency where the skin depth is much smaller than the chamber wall thickness, the transverse resistive-wall impedance is proportional to $1/\omega^{1/2}$. This region may be called as the conventional region. At lower frequency, there is the unconventional frequency region where the skin depth is larger than the wall thickness, but typically less than 10 times the wall thickness. In this region, the transverse resistive-wall impedance becomes proportional to $1/\omega$, not $1/\omega^{1/2}$. Thus the impedance increases more rapidly as the frequency goes down. In this region, the whole image current still runs on the thin chamber wall, and thus wake-fields do not leak out (in other words, perfectly shielded). Then, there is the extreme thin wall region at low frequency where the skin depth is much larger than the wall thickness and wake-fields can easily leak out of the chamber and thus the impedance drops rapidly, proportional to the frequency itself, as the frequency goes down.

The growth rate of vertical beam instabilities due to the MR stainless-steel chamber was re-estimated using these new results. The vertical tune was also changed to 20.793 in the new calculation, resulting in further increase in the growth rate. Due to the synergy effect of the two changes, the growth rate of vertical beam instabilities is nearly doubled from the previous estimate. The vertical growth rate as a function of the ramping time is plotted in Fig. 14. At the injection energy of 3 GeV, the growth rate now becomes more than 2 kHz.

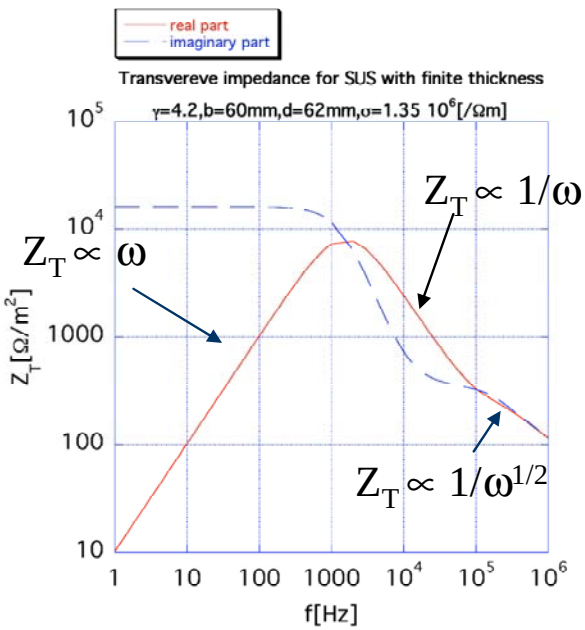

Figure 13: Transverse impedance of the MR stainless-steel chamber and the three different regions of frequency dependency.

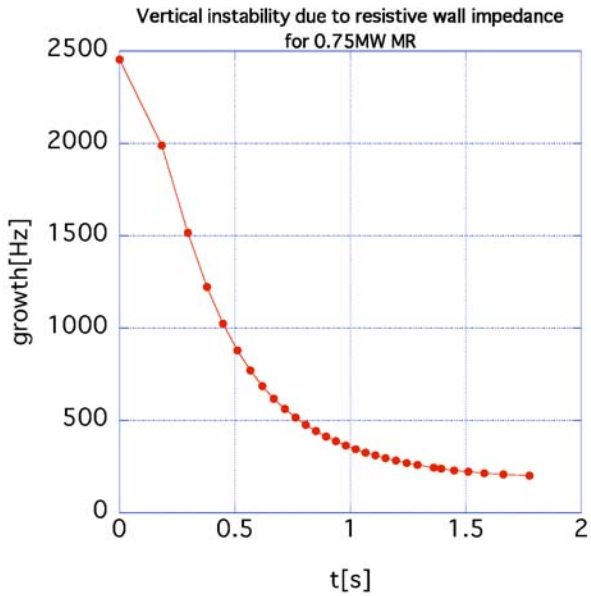

Figure 14: The vertical growth rate due to the MR stainless-steel chamber as a function of the ramping time.

EXCITERS AS DAMPERS

There are two exciters installed in the MR for transverse tune measurements (horizontal and vertical, respectively). The photo of the vertical exciter is shown in Fig. 15. Study is under way to use these exciters as dampers to damp transverse beam instabilities at the MR. The calculation shows that the input power of 1kW can create a 7.6kV kick per turn to a beam.

Figure 15: Horizontal exciter of the MR.

REFERENCES

[1] Y. Yamazaki, PAC2003, p.576.
[2] M. Tigner and A. Chao, "Handbook of Accelerator Physics and Engineering", 1999, World Scientific River Edge, NJ.
[3] H. Hahn, BNL/SNS Tech. Note No. 140, 2004.
[4] W. Zhang et al., EPAC2004, p.1810.
[5] A. Shishlo et al., ICAP2006, p.53.
[6] B. Zotter, CERN-AB-2005-043, 2005.
[7] E. Métral, CERN-AB-2005-084, 2005.